Earth and Planetary Science Letters 500 (2018) 86–96

Contents lists available at ScienceDirect

Earth and Planetary Science Letters

www.elsevier.com/locate/epsl

The influence of deep mantle compositional heterogeneity on Earth's thermal evolution

Mingming Li [a,*], Allen K. McNamara [b]

[a] Arizona State University, School of Earth and Space Exploration, PO Box 876004, Tempe, AZ 85287-6004, USA
[b] Michigan State University, Department of Earth and Environmental Sciences, Natural Science Building, East Lansing, MI 48824, USA

ARTICLE INFO

Article history:
Received 5 November 2017
Received in revised form 16 June 2018
Accepted 5 August 2018
Available online 16 August 2018
Editor: B. Buffett

Keywords:
thermal evolution
compositional heterogeneity
thermochemical piles
lowermost mantle

ABSTRACT

The seismically-observed large low shear velocity provinces in the Earth's lowermost mantle have been hypothesized to be caused by thermochemical piles of compositionally distinct, more-primitive material which may be remnants of Earth's early differentiation. However, one critical question is how the Earth's thermal evolution is affected by the long-term presence of the large-scale compositional heterogeneity in the lowermost mantle. Here, we perform geodynamical calculations to investigate the time evolution of the morphology of large-scale compositional heterogeneity and its influence on the Earth's long-term thermal evolution. Our results show that a global layer of intrinsically dense material in the lowermost mantle significantly suppresses the CMB heat flux, which leads to faster cooling of the background mantle relative to an isochemical mantle. As the background mantle cools, the intrinsically dense material is gradually pushed into isolated thermochemical piles by cold downwellings. The size of the piles also decreases with time due to entraining of pile material into the background mantle. The morphologic change of the accumulations of intrinsic dense material eventually causes a gradual increase of CMB heat flux, which significantly reduces the cooling rate of Earth's mantle.

1. Introduction

Understanding the Earth's thermal evolution is one the most important problems in Earth Sciences. The thermal evolution of Earth's mantle dictates the partial melting and degassing processes occurring in the uppermost mantle which have great influences on climate change and atmospheric evolution. One key factor that controls the thermal evolution of the Earth's mantle is the core–mantle boundary (CMB) heat flux, which is largely determined by the lowermost mantle structure and dynamics.

Seismic observations have revealed two large low shear velocity provinces (LLSVPs) in Earth's lowermost mantle, surrounded by regions with much higher seismic velocities that are suggested to be ancient subducted cold slabs (e.g., Li and Romanowicz, 1996; Ritsema et al., 2004). One hypothesis for the origin of LLSVPs is that they are caused by large-scale, compositionally-distinct material that may be remnants of Earth's early differentiation (e.g., Labrosse et al., 2007). The large-scale compositional heterogeneity may have been pushed by convection into hot but intrinsically dense thermochemical piles that cause the LLSVPs (Davaille, 1999; Li and Zhong, 2017; McNamara and Zhong, 2005; Tackley, 1998; Zhang et al., 2010). The thermochemical piles are expected to act as thermal insulators (Nakagawa and Tackley, 2004), beneath which the CMB heat flux is much lower than that outside piles (Zhang and Zhong, 2011). Thus, the lateral extent of thermochemical piles on the CMB significantly controls the CMB heat flux.

The morphology of thermochemical piles is expected to change with time. Firstly, changing mantle convection currents will act to push the piles away from regions of downwelling and into regions of upwelling. Furthermore, and of specific relevance to this paper, the total geographic area of core–mantle boundary surface that thermochemical piles will cover is expected to decrease with time. This primarily occurs for two reasons that control topographic relief of piles (lower topographic relief leads to a more layer-like morphology that covers more CMB surface area, and vice versa). Firstly, as the Earth cools and the mantle's effective Rayleigh number becomes smaller, piles are more viscously coupled to background mantle flow and therefore obtain higher topographic relief (e.g., Tackley, 1998). Secondly, as time passes, the effective density difference between thermochemical piles and the background mantle decreases, making the piles effectively less-dense and therefore obtain higher topographic relief. This occurs for two reasons. With time, thermochemical piles and background mantle continually exchange material via entrainment (e.g., Davaille, 1999; Deschamps et al., 2011; Li et al., 2014), which acts to reduce

* Corresponding author.
E-mail address: Mingming.Li@asu.edu (M. Li).

https://doi.org/10.1016/j.epsl.2018.08.009
0012-821X/

the intrinsic density contrast between them (and incidentally also makes piles smaller with time (e.g., Davaille, 1999; Li et al., 2014)). Also, cooling is more efficient for background mantle than for thermochemical piles. If starting with an initially hot temperature for the entire system, an increasing temperature differential between piles and background mantle develops through time because the background mantle cools faster. Therefore, the difference in thermal expansion between piles and background mantle increases with time (i.e., the background mantle gets thermally denser than piles), which acts to reduce the effective density contrast between them.

Here, we investigate how the presence of thermochemical piles in the lowermost mantle can affect the Earth's thermal evolution. In an isochemical convection system that lacks thermochemical piles, the temperature of the entire mantle is predicted to generally decrease in a monotonic manner as a function of time for most of Earth's history (e.g., Christensen, 1985; Davies, 1993; Honda, 1995; McNamara and Keken, 2000; Schubert et al., 1980). This is due to the decreasing concentrations of radioactive heat-producing elements and secular cooling of the mantle through time. Note that this monotonic temperature decrease can sometimes be preceded by an early, transient temperature increase, particularly for relatively low initial temperatures (e.g., Christensen, 1985; Davies, 1980; Franck, 1998). In this study, we introduce a denser mantle component in the lowermost mantle of an initially uniform hot Earth. We find that this denser material will evolve from a flat layer to discrete thermochemical piles as the mantle cools with time. We find that although the initial global layer of intrinsically dense material on the CMB significantly reduces the CMB heat flux, which leads to rapid cooling of Earth's background mantle, the transition of this dense layer to discrete thermochemical piles and the reduction of pile size due to entrainment lead to eventual increases of CMB heat flux, which in turn cause a reduction of cooling rate and possibly temperature increase of Earth's upper mantle with time. Thus, the presence of a thermochemical layer may initially cool the upper mantle quicker than would be expected for an isochemical mantle. This is followed by a reduced cooling rate or possibly heating up of the upper mantle as the dense layer transitions into discrete thermochemical piles.

2. Method

We perform both isochemical and thermochemical numerical calculations to study thermal evolution of Earth's mantle. The following non-dimensional equations of conservation of mass, momentum and energy are solved under the Boussinesq approximation:

$$\nabla \cdot \vec{u} = 0, \tag{1}$$

$$-\nabla P + \nabla \cdot (\eta \dot{\epsilon}) = \xi^{-3} Ra(T - BC)\hat{r}, \tag{2}$$

$$\frac{\partial T}{\partial t} + (\vec{u} \cdot \nabla)T = \nabla^2 T + Q, \tag{3}$$

where, $\vec{u}$ is the velocity, P is the dynamic pressure, η is the viscosity, $\dot{\epsilon}$ is the strain rate, Ra is the Rayleigh number, T is the temperature, B is the buoyancy number, C is the compositional concentration, $\hat{r}$ is the unit vector in radial direction, t is the time, and Q is the internal heat generating rate. The spatial dimension is non-dimensionalized by the Earth's radius, not mantle thickness. Therefore, we include $\xi = D/R_e$, where D is the thickness of Earth's mantle and R_e is the Earth's radius. All parameters in equations (1)–(3) are non-dimensional. The above equations are solved using the CitcomCU code (Zhong, 2006).

The Rayleigh number Ra in equation (2) is defined as:

$$Ra = \frac{\rho g \alpha \Delta T D^3}{\eta_0 \kappa}, \tag{4}$$

Table 1
Physical parameters and reference values.

Parameters	Symbol	Value
Earth's radius	R	6370 km
Thickness of Earth's mantle	D	2890 km
Gravitational acceleration	g	9.8 m/s^2
Density of background mantle	ρ	3300 kg/m^3
Thermal expansivity	α	1×10^{-5} K^{-1}
Temperature difference between CMB and surface	ΔT	2500 K
Reference viscosity	η_0	2×10^{20}, 4×10^{20} Pa s
Thermal diffusivity	κ	1×10^{-6} m^2/s

where, ρ, g, α, ΔT, η_0 and κ are dimensional parameters for density of the background mantle, gravitational acceleration, thermal expansivity, potential temperature difference between CMB and surface, reference viscosity at temperature $T = 0.6$ (non-dimensional), and thermal diffusivity, respectively. Table 1 lists the reference values of physical parameters used in this study.

The buoyancy number B in equation (2) is defined as the ratio between intrinsic density anomaly and density anomaly due to thermal expansion:

$$B = \frac{\Delta \rho}{\rho \alpha \Delta T}, \tag{5}$$

where, $\Delta\rho$ is intrinsic excess density of pure pile material with respect to background mantle material. Using reference values in Table 1, the buoyancy number of 0.4, 0.8 and 1.2 are scaled to intrinsic density anomalies of 1%, 2% and 3%, respectively. The composition concentration C in equation (2) represents the concentration of the intrinsic dense material within one element of the computational domain in this study. The background mantle regions have $C = 0$, regions with pure intrinsic dense material have $C = 1$, and regions with a mixture of background mantle material and intrinsic dense material have $0 < C < 1$.

The viscosity depends on both temperature and depth. The temperature dependent viscosity is $\eta_T = \exp[A(0.6 - T)]$, where A is activation parameter which controls the amount of viscosity changes due to changes in temperature. For most of our cases, A is 9.21 in both upper and lower mantles, which leads to 10,000 viscosity contrast between lowest ($T = 0$) and the highest temperature ($T = 1$). In addition, there is a 50× viscosity increase from upper mantle to lower mantle across the 670-km discontinuity.

The whole mantle dynamics is modeled in a spherical annulus geometry (Hernlund and Tackley, 2008). The radius of inner (representing the CMB) and outer (representing the surface) layer of the model domain are $r_i = 0.55$ and $r_o = 1.0$, respectively. The model domain is divided into 1280 × 128 (longitudinal and radial, respectively) elements. Both the surface and the CMB have free-slip velocity boundary condition. The temperature boundary condition is isothermal on the surface ($T = 0$) and the CMB ($T = 1$). The model is both internally and basal heated.

The temperature initial condition for most cases is $T = 0.72$ throughout the domain with small sinusoidal perturbations superimposed to enhance convection at the beginning. For thermochemical models, we also initially introduced a global layer of intrinsically dense material at the bottom the mantle. The composition advection is performed using ~3.28 million tracers (~20 tracers per element on average) using the ratio tracer method (Tackley and King, 2003).

The Earth's thermal evolution is influenced by factors such as the internal heating rate, vigor of mantle convection, the nature of plate motion in the early Earth (e.g., Davies, 2009; Korenaga, 2006), phase transition at Earth's transition zone (Davies, 2008), surface magmatism (e.g., Nakagawa and Tackley, 2012), and the supercontinent cycles (e.g., Coltice et al., 2007; Lenardic et al., 2011;

Table 2
Cases used in this study.

Case	Ra	A	Q_p	Q_{bg}	B	d (km)	T_{ini}	dT/dt (K/Gyr)
ISO1	5e7	9.21	60	60	N/A	N/A	0.72	N/A
TC1.1	5e7	9.21	60	60	0.8	300	0.72	75
TC1.2	5e7	9.21	60	60	0.4	300	0.72	N/A
TC1.3	5e7	9.21	60	60	1.2	300	0.72	51
TC1.4	5e7	9.21	60	60	0.8	150	0.72	46
TC1.5	5e7	9.21	60	60	0.8	600	0.72	74
ISO2	5e7	9.21	40	40	N/A	N/A	0.72	N/A
TC2.1	5e7	9.21	40	40	0.8	300	0.72	65
TC2.2	5e7	9.21	23.7	237	0.8	300	0.72	64
ISO3	1e8	9.21	60	60	N/A	N/A	0.72	N/A
TC3	1e8	9.21	60	60	0.8	300	0.72	50
ISO4	5e7	11.51	60	60	N/A	N/A	0.72	N/A
TC4	5e7	11.51	60	60	0.8	300	0.72	69
ISO5.1	5e7	9.21	60	60	N/A	N/A	0.64	N/A
TC5.1	5e7	9.21	60	60	0.8	300	0.64	51
ISO5.2	5e7	9.21	60	60	N/A	N/A	0.80	N/A
TC5.2	5e7	9.21	60	60	0.8	300	0.80	52

Ra: Rayleish number; A: activation parameter for temperature dependent viscosity below 100 km depth, and A is 9.21 above 100 km depth for all cases; Q_p: internal heating rate of intrinsic dense material; Q_{bg}: internal heating rate of background mantle material; B: buoyancy number; d: initial thickness of compositional heterogeneity; dT/dt: the average increasing rate of T_{300} (the ambient upper mantle temperature at 300 km depth) within the first ~10 transit times (~600 Myr) after T_{300} reaches a minimum value; T_{ini}: initial mantle temperature.

Phillips and Bunge, 2005; Zhong and Gurnis, 1993). A comprehensive understanding of Earth's thermal evolution is beyond the scope of this study. Here, we focus on the morphologic change of the large-scale compositional heterogeneities and its effects on upper mantle thermal evolution. We perform 5 sets of calculations (Table 2). Each set of calculations consist of one isochemical model and one or more corresponding thermochemical models with the same parameters as the isochemical models but also containing compositional heterogeneity. By comparing the results of the thermochemical calculations with the corresponding isochemical calculation, we investigate the effects of compositional heterogeneity on thermal evolution of Earth's mantle. The internal heating rate and the CMB temperature are kept constant in each model, which allow us to focus on understanding how morphologic changes of compositional heterogeneity affects the Earth's thermal evolution.

In this study, we quantify and show the changes of temperature in the uppermost mantle (at 300 km depth) because it is most relevant to the partial melting and degassing processes of the Earth. We define the "ambient temperature" as the horizontally averaged temperature in regions with $T > T_{ave}$ (e.g., excluding cold downwelling regions), where T_{ave} is the horizontally averaged temperature. Below, we denote the ambient upper mantle temperature at 300 km depth as T_{300}.

We use two different approaches to scale model time to geological time. One direct way is through diffusion time in which the model time is dimensionalized by:

$$t_g = \left(\frac{R_e^2}{\kappa}\right) * t', \tag{6}$$

where t_g and t' are the dimensional diffusion time (e.g., geological time) and the dimensionless time (e.g., model time), respectively. However, precautions must be taken when interpreting the dimensional diffusion time in this study. Firstly, the diffusion time varies significantly with the effective Rayleigh number of the mantle, which is not well constrained for the true Earth, especially for the Earth's early history. If the mantle viscosity in models is higher than that of the true Earth, the diffusion time can be significantly over-estimated. Secondly, the compositional heterogeneities are pushed into thermochemical piles by downwelling slabs and as a result, the morphology of the piles is strongly controlled by the surface velocity. The surface velocity in our models is small (~0.7 cm/yr for the 1st set of models), because the lithosphere is very viscous due to use of temperature dependent viscosity. As a result, it takes very long diffusion time for the global layer of dense material to be pushed into isolated piles. Generating self-consistent Earth-like subduction remains challenging in geodynamic modeling, and the plate motion in Earth's early history is poorly constrained. Therefore, we do not aim to produce an Earth-like plate tectonics in this study. However, to better scale with the true Earth, we also measure the model time in terms of the transit time (Christensen and Hofmann, 1994; Zhong and Gurnis, 1993). The number of transit times is given by:

$$t_{transit} = \int_0^t \frac{\overline{u}(t')}{\xi} dt', \tag{7}$$

where t is the non-dimensional time, and $\overline{u}(t')$ is the average absolute velocity on the surface at non-dimensional time t' and ξ is defined previously in equation (2). By definition, 1 transit time equals to the time takes for slabs to sink from the surface to the CMB. All models in this study are run for ~140 transit time. For reference, the transit time is plotted against the dimensional diffusion time for all models in Supplementary Information Fig. S1.

3. Results

3.1. Results for the reference cases

We first compare the results for two reference cases: the isochemical case ISO1 and the thermochemical case TC1.1. For both cases, the Rayleigh number is $Ra = 5 \times 10^7$, the internal heating rate is $Q = 60$, and the activation coefficient for temperature-dependence of viscosity is $A = 9.21$ (Table 2). Both cases have the same initial temperature condition. A global layer of intrinsically dense material is initially introduced in the lowermost 300 km mantle for case TC1.1, with a buoyancy number of $B = 0.8$.

Fig. 1 shows a time series of snapshots of temperature field for case ISO1 (Fig. 1a–d) and case TC1.1 (Fig. 1e–h) and composition field for case TC1.1 (Fig. 1i–l). In case ISO1, the cold downwellings sink all the way to the CMB and hot mantle plumes form from the basal thermal boundary layer (Fig. 1a–d). In case TC1.1, the CMB is completely covered by a global intrinsic dense layer during the early stage of the calculation ($t < t_1$, Fig. 1i). Gradually, the global layer of dense material in case TC1.1 is pushed into isolated thermochemical piles, and the size of the piles decrease with time because of entrainment into the background mantle (e.g., Fig. 1f–h, 1j–l). The composition C of the piles decreases with time due to mixing of background mantle material into the piles (Fig. 1i–l). The background temperature is generally lower for case TC1.1 than case ISO1 at $t = t_1$ and $t = t_2$ due to layer of dense material thermally insulating the background mantle from the core. As piles later get entrained into the background mantle, the temperature of the two cases becomes more similar, from $t = t_3$ to $t = t_4$.

As shown in Fig. 2, the two cases show characteristic differences in both the evolution of the CMB heat flux and the surface heat flux. The CMB heat flux for case ISO1 remains nearly constant throughout the calculation (dashed red curve), whereas it continually increases with time in case TC1.1 (dashed black curve) with the increase in the fraction of exposed CMB area which is not covered by pile material (solid gray curve). The CMB heat flux is similar for both cases after most pile material is stirred into

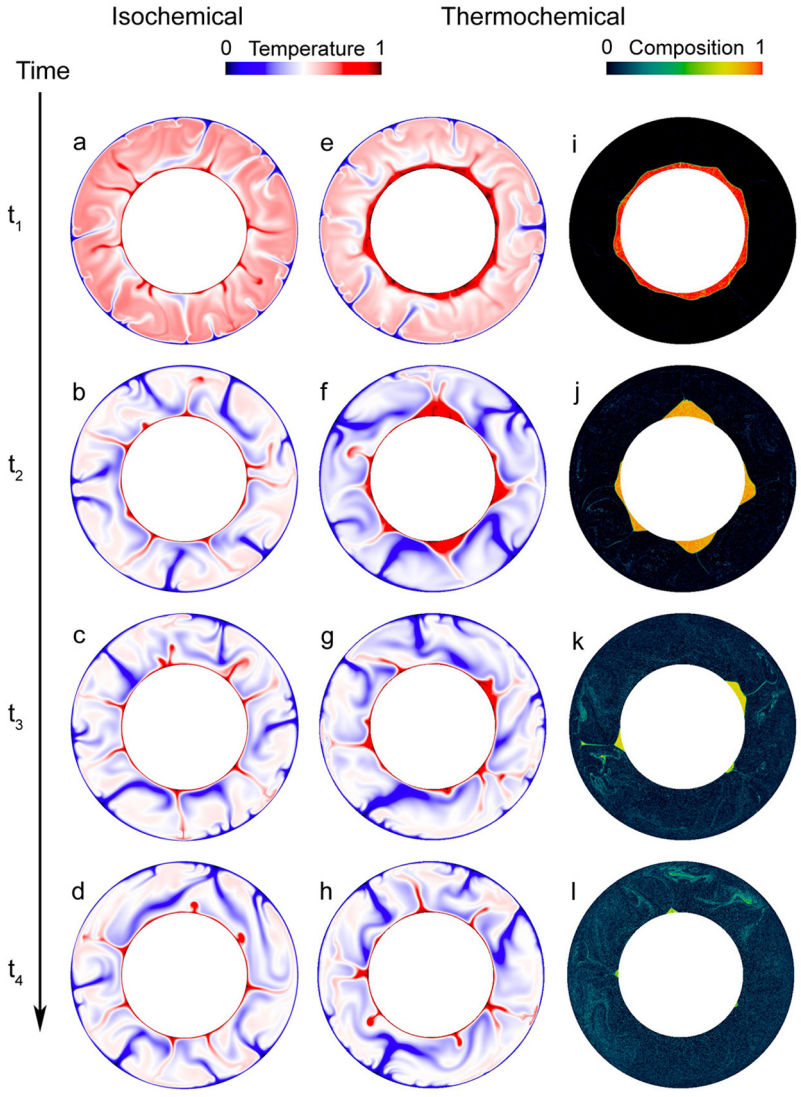

Fig. 1. Temperature field for case ISO1 (**a–d**) and case TC1.1 (**e–h**), and composition field for case TC1.1 (**i–l**) at 4 ($t = t_1$), 44 ($t = t_2$), 90 ($t = t_3$), and 116 ($t = t_4$) transit time. (For interpretation of the colors in the figure(s), the reader is referred to the web version of this article.)

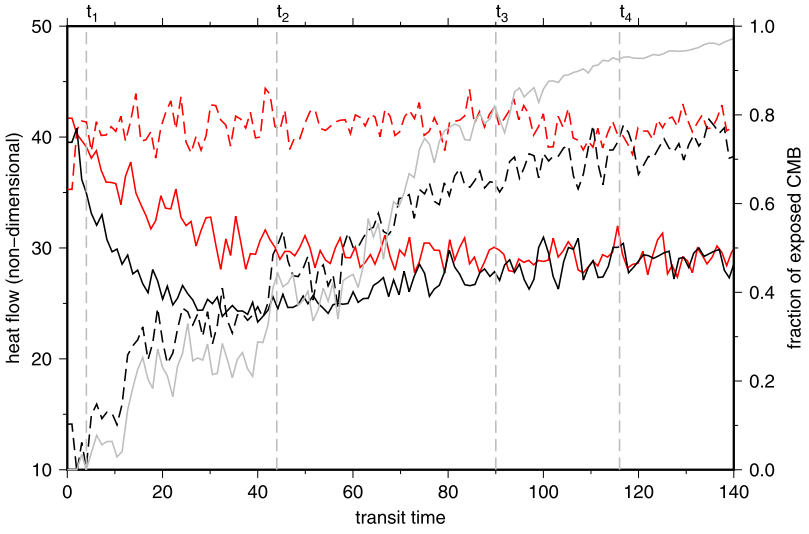

Fig. 2. Time evolution of the surface heat flow (solid red for case ISO1 and solid black for case TC1.1) and CMB heat flow (dashed red for case ISO1 and dashed black for case TC1.1), and the fraction of exposed CMB not covered by intrinsic dense material for case TC1.1 (solid gray). The dashed vertical gray lines show 4 times at 4 ($t = t_1$), 44 ($t = t_2$), 90 ($t = t_3$), and 116 ($t = t_4$) transit time.

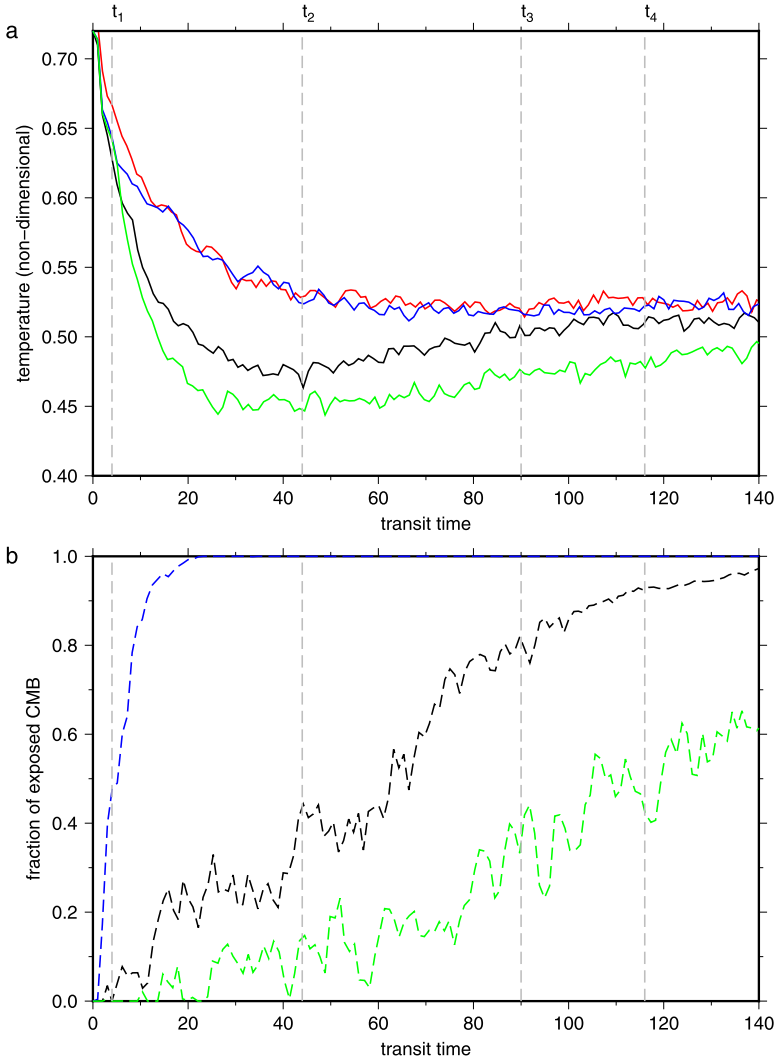

Fig. 3. a, Ambient upper mantle temperature at 300 km depth (T_{300}) as a function of time for cases ISO1 (red), TC1.1 (black), TC1.2 (blue), and TC1.3 (green). The dashed vertical gray lines show 4 times: 4 ($t = t_1$), 44 ($t = t_2$), 90 ($t = t_3$), and 116 ($t = t_4$) transit time. **b**, Time evolution of the fraction of exposed CMB not covered by intrinsic dense material for cases TC1.1 (black), TC1.2 (blue) and TC1.3 (green). Cases TC1.2 and TC1.3 have different buoyancy number for the intrinsic dense material than case TC1.1.

the background mantle in case TC1.1 ($t > t_4$). For both cases, the surface heat flux is high during the early stage of the calculation ($t < t_1$). However, the trend of the surface heat flux for case ISO1 decreases monotonically with time (solid red curve), whereas for case TC1.1, it first decreases faster than that in case ISO1 until it reaches minimum at $t \sim t_2$ and then gradually increases with time (solid black curve). After $t \sim t_4$, the surface heat flux for two cases become similar.

As expected, the background temperatures for the two cases also evolve differently with time. The evolution of T_{300} (which denotes the ambient upper mantle temperature at 300 km depth) for both cases is shown in Fig. 3a. For case ISO1, it decreases monotonically with time (Fig. 3a, red curve). In addition, the cooling rate is high during the early stage of the calculation and it decreases with time until the temperature reaches thermal equilibrium. In contrast, the T_{300} in case TC1.1 (Fig. 3a, black curve) is strongly affected by fraction of the exposed CMB (Fig. 3b, dash black curve). It first decreases rapidly when the CMB is covered by global layer of dense material (e.g., Fig. 1i). At $t = t_2$, it reaches its minimum value of ~0.464. After $t = t_2$, the T_{300} gradually increases with time, accompanied by increasing amount of exposed CMB area. At $t = t_3$, it increases to ~0.506 when about 80% of CMB is exposed. At $t = t_4$, it increases to ~0.511 when more than 95% of CMB is exposed. Finally, all intrinsic dense material is mixed into the background mantle, and the T_{300} becomes identical to that of case ISO1.

In summary, we find that the CMB heat flux is significantly affected by the morphologic change of the large-scale compositional heterogeneity in the lowermost mantle, which in turn strongly affects the background mantle temperature and the surface heat flux. Whereas the T_{300} for case ISO1 decreases monotonically with time, in thermochemical case TC1.1, it first decreases to minimum and then starts to increase with time.

3.2. *Effects of intrinsic density anomaly of compositional heterogeneity*

In this section, we explore the effects of the intrinsic density anomaly of the large-scale compositional heterogeneity on our results. In case TC1.2, the buoyancy number of intrinsically dense material is decreased to $B = 0.4$ (Table 2). Similar to case TC1.1, the global intrinsically dense layer on the CMB leads to rapid cooling of the ambient upper mantle during the early stage of the calculation (Fig. 3a, blue curve). However, the pile material above the CMB is completely stirred into the background mantle after only 20 transit times (Fig. 3b, dashed blue curve), which is much shorter than that for case TC1.1 (~140 transit time). After 20 transit times, the evolution of T_{300} becomes the same as the isochemical case ISO1 (Fig. 3a).

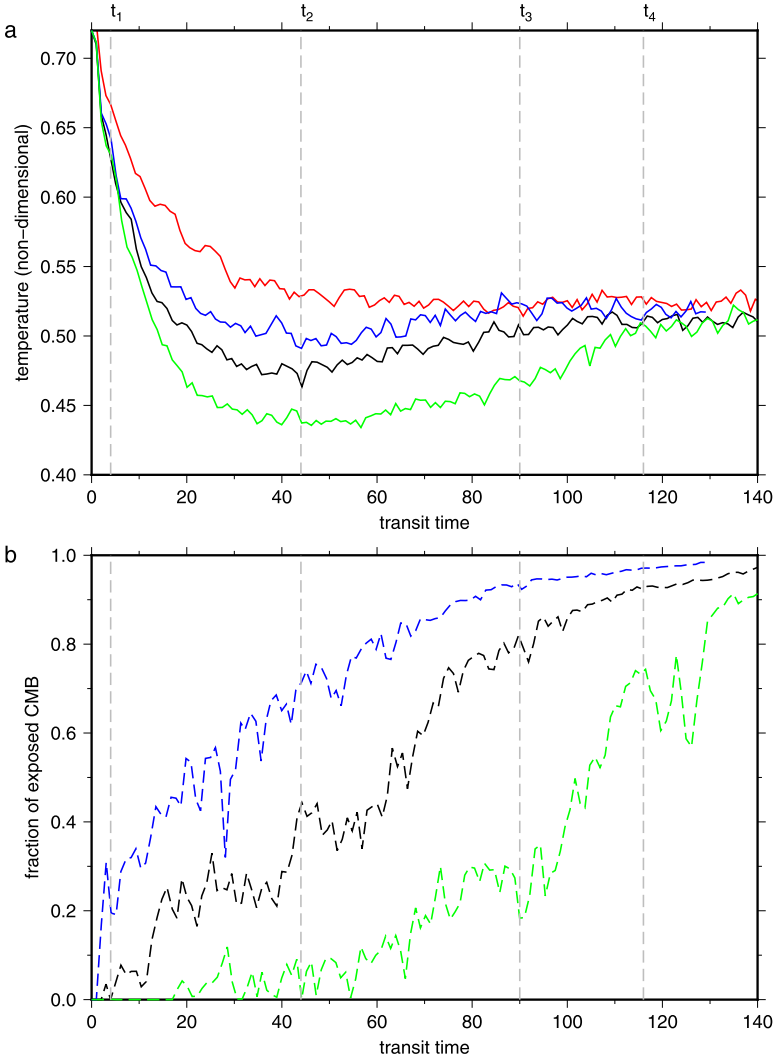

Fig. 4. a, Ambient upper mantle temperature at 300 km depth (T_{300}) as a function of time for cases ISO1 (red), TC1.1 (black), TC1.4 (blue), and TC1.5 (green). The dashed vertical gray lines show 4 times at 4 ($t = t_1$), 44 ($t = t_2$), 90 ($t = t_3$), and 116 ($t = t_4$) transit time. **b**, Time evolution of the fraction of exposed CMB not covered by intrinsic dense material for cases TC1.1 (black), TC1.4 (blue) and TC1.5 (green). Cases TC1.4 and TC1.5 have different initial thickness of the intrinsic dense material than case TC1.1.

In case TC1.3, the buoyancy number of intrinsic dense material is increased to $B = 1.2$ (Table 2). The T_{300} in case TC1.3 is, for most of the time, much lower than case TC1.1, but it also first decreases rapidly until it reaches its minimum and then gradually increases with time (Fig. 3a, green curve). The increased intrinsic density of compositional heterogeneity in the lowermost mantle significantly reduces the entrainment rate of the pile material. Therefore, after 140 transit times, only ~60% CMB is exposed (Fig. 3b, dashed green curve) and the T_{300} increases slowly (Fig. 3a, green curve).

3.3. Effects of initial thickness of the global layer of compositional heterogeneity

In this section, we explore how the initial volume of the intrinsically dense material affects our results. Fig. 4a shows the time evolution of T_{300} for cases ISO1, TC1.1, TC1.4 and TC1.5 and Fig. 4b shows the evolution of the fraction of exposed CMB area for cases TC1.1, TC1.4 and TC1.5. In case TC1.4, the initial thickness of intrinsic dense material is reduced to 150 km. As a result, the fraction of exposed CMB area is larger than case TC1.1. In addition, the T_{300} is generally higher than case TC1.1 for most of the time (Fig. 4a, blue curve); but it evolves in the same manner as in case TC1.1: first decreases rapidly to minimum and then gradually increases with time.

In case TC1.5, the initial thickness of intrinsic dense material is increased to 600 km. In this calculation, the T_{300} is much lower than case TC1.1 for most of the time (Fig. 4a, green curve), and the CMB is covered by a global layer of intrinsically dense compositional heterogeneity for a longer time than in case TC1.1 (Fig. 4b, dashed green curve). The T_{300} in case TC1.5 experiences rapid cooling in the first 20 transit times, and it reaches minimum at ~40–50 transit times. After that, the T_{300} gradually increases with time, accompanied by gradual increases of the fraction of exposed CMB area. At ~130 transit times, most of the pile material in case TC1.5 is stirred into the background mantle, and the T_{300} becomes similar to that in cases TC1.1 and ISO1.

3.4. Influence of internal heating rate

In the second set of calculations, both the isochemical model of case ISO2 and the thermochemical model of case TC2.1 have internal heating rate of $Q = 40$ (Table 2), which is 2/3 of that in the first set of calculations (i.e., cases ISO1 and TC1.1-1.5). In case TC2.2, the global average internal heating rate of $Q = 40$ is redistributed to the intrinsically dense material and background material, with the intrinsically dense material having 10 times more heat generation than the background mantle material (Table 2).

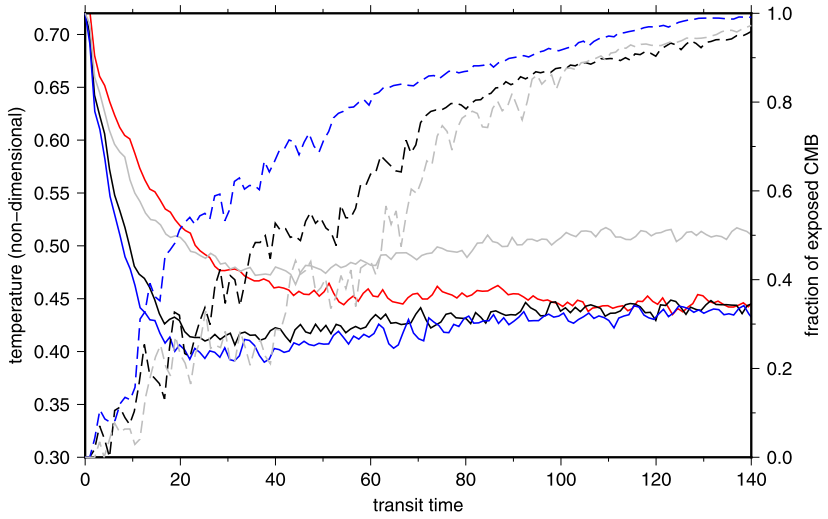

Fig. 5. Time evolution of the ambient upper mantle temperature at 300 km depth (T_{300}) for cases ISO2 (solid red), TC2.1 (solid black), TC2.2 (solid blue) and TC1.1 (solid gray), and the fraction of exposed CMB not covered by intrinsic dense material for cases TC2.1 (dashed black), TC2.2 (dashed blue) and TC1.1 (dashed gray). For cases ISO2 and TC2.1, the internal heating rate is 40. For case TC2.2, the intrinsic dense material has 10 times more internal heating rate than the background mantle material, while the volume average of the internal heating rate is the same as case TC2.1.

Fig. 5 shows the evolution of ambient upper mantle temperature for the second set of calculations. As expected, the mantle temperature is lower than the first set of calculations (e.g., solid gray curve in Fig. 5 shows the T_{300} for case TC1.1), because of reduced internal heating rate. However, the trend for the evolution of the T_{300} is similar to that of the first set of calculations. For the isochemical case ISO2 (red curve), T_{300} decrease rapidly at the beginning and become stable after about 80 transit times; while for the thermochemical case TC2.1, T_{300} (solid black curve) first decreases to their minimum values with a faster cooling rate than case ISO2, then gradually increases with time accompanied with increasing amount of exposed CMB area (dashed black curve), and finally become relatively stable with similar values as that of case ISO2.

In case TC2.2, during the early stage of the calculation, low internal heating rate in background mantle results in faster cooling of the background mantle than that of case TC2.1 (Fig. 5). However, high internal heating rate of the intrinsically dense material results in higher temperature, lower excess density anomaly, and faster entrainment of the thermochemical piles of dense material (e.g., compare dashed blue curve for case TC2.2 and dashed black curve for case TC2.1). As the intrinsically dense material is stirred into the background mantle, the internal heating rate of the background mantle material increases. The enrichment of heat producing elements in the intrinsically dense material with respect to the background mantle material has only minor effects on the long-term evolution of upper mantle ambient temperature (Fig. 5).

3.5. Influence of Rayleigh number

In the third set of calculations, the Rayleigh number for both isochemical case ISO3 and thermochemical case TC3 is increased to $Ra = 10^8$. The background temperature for this set of cases with higher Rayleigh number is generally lower than that in the first set of calculations (e.g., comparing the solid gray curve for case TC1.1 and the solid black curve for case TC3 in Fig. 6), which is consistent with previous studies showing that the average background mantle temperature is inversely proportional to the Rayleigh number when internal heating is not zero (Sotin and Labrosse, 1999). Similar to previous sets of calculations, we find that the morphologic changes of compositional heterogeneity in the lowermost mantle significantly affect the evolution of the T_{300} (Fig. 6). For the thermochemical case TC3, T_{300} reaches its minimum value after about 40 transit times and then gradually increases with time until most of the intrinsically dense material is stirred into the background mantle.

3.6. Influence of temperature dependent viscosity

In the fourth set of calculations, we explored the effects of temperature-dependent viscosity on our results. Temperature-dependent viscosity in the top thermal boundary layer has been found to have big effects on surface mobility, which could significantly affect Earth's thermal evolution (e.g., Christensen, 1985). Since our goal in this study is to isolate the effects of thermochemical convection in Earth's lowermost mantle on the thermal evolution of Earth's mantle, we keep the temperature dependent viscosity the same as that of the first set of our calculations in the first 100 km of the upper mantle, while explored different temperature dependent viscosity below 100 km depth. In case ISO4 and TC4, the activation efficiency A is increased to 11.51 below 100 km depth, leading to a maximum of $10^5\times$ viscosity contrast due to changes of temperature. Again, we find that the evolution of large-scale compositional heterogeneity in the lowermost mantle has important effects on upper mantle temperature. While the T_{300} monotonically decreases with time for case ISO4, for case TC4 it first decreases rapidly until reaches its minimum value and then gradually increases with time, accompanied by an increasing fraction of exposed CMB area (Fig. 7). Note that case TC4 has higher T_{300} than the reference case TC1.1, consistent with that case TC4 has generally larger fraction of exposed CMB area than case TC1.1.

3.7. Influence of initial temperature condition

In the cases discussed above, the initial mantle temperature is set to be $T = 0.72$. In the fifth set of calculations, we explore the effects of different initial mantle temperature on our results. In cases ISO5.1 and TC5.1, the initial mantle temperature is reduced to $T = 0.64$, while in cases ISO5.2 and TC5.2, we increase the initial temperature to $T = 0.8$ (Table 2). Again, we found that the T_{300} decreases monotonically for the isochemical cases ISO5.1 and ISO5.2, while it first decreases to minimum and then increases with time for the thermochemical cases TC5.1 and TC5.2 (Fig. 8a, b). Compared to case TC1, a higher (lower) initial temperature in case TC5.2 (TC5.1) leads to faster (slower) decrease of T_{300}

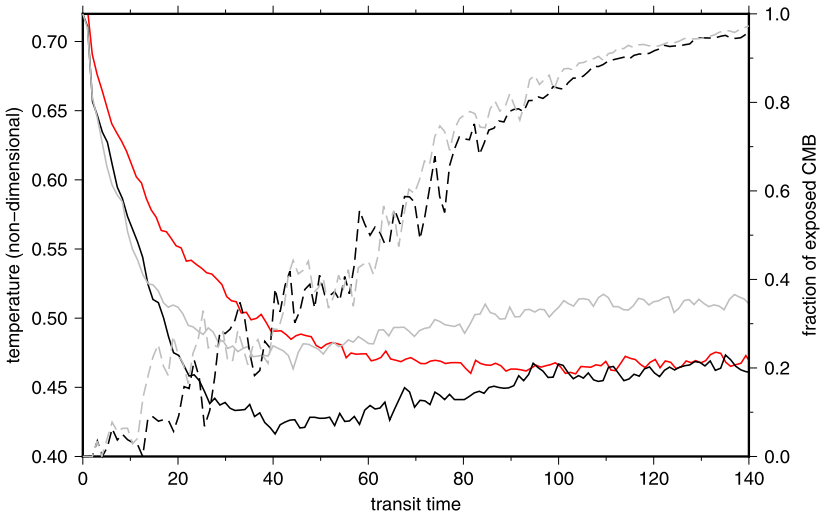

Fig. 6. Time evolution of the ambient upper mantle temperature at 300 km depth (T_{300}) for cases ISO3 (solid red), TC3 (solid black), and TC1.1 (solid gray), and the fraction of exposed CMB not covered by intrinsic dense material for cases TC3 (dashed black) and TC1.1 (dashed gray). The Rayleigh number is 1e8 for cases ISO3 and TC3.

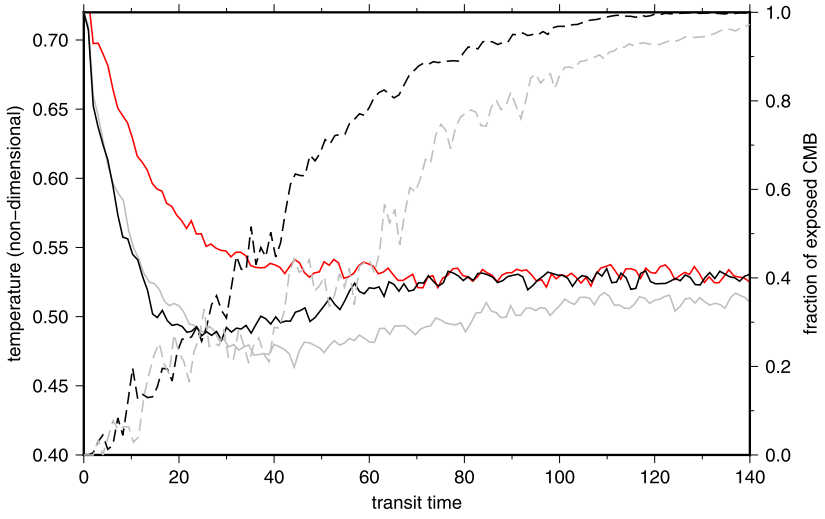

Fig. 7. Time evolution of the ambient upper mantle temperature at 300 km depth (T_{300}) for cases ISO4 (solid red), TC4 (solid black), and TC1.1 (solid gray), and the fraction of exposed CMB not covered by intrinsic dense material for cases TC4 (dashed black) and TC1.1 (dashed gray). The temperature dependent viscosity at deeper than 100 km depths is enhanced for both cases ISO4 and TC4 with an activation parameter $A = 11.51$.

until it reaches minimum values (Fig. 8a, b). Interestingly, for cases TC1.1, TC5.1 and TC5.2, the minimum values of the T_{300} and the subsequent thermal evolutions after the T_{300} reaches minimum are similar (Fig. 8a, b), indicating that the initial temperature has no or little effects on the long-term thermal evolution of Earth's mantle. This finding is consistent with previous parameterized models (e.g., Christensen, 1985) and numerical models (e.g., Nakagawa and Tackley, 2012) which showed that no matter if the Earth started cool or hot, it would reach similar thermal state after some time.

4. Discussion and conclusion

Here, we study the morphologic changes of the large-scale compositional heterogeneity in the lowermost mantle and their effects on the upper mantle temperature. In case TC1.2, the short-term presence of the large-scale compositional heterogeneity in the lowermost mantle has little effects on the long-term thermal evolution in the upper mantle (Fig. 3a, red curve). For other thermochemical cases, the temperature of upper mantle first decreases with time. After it reaches the minimum value, it then gradually increases with time and finally reaches quasi-equilibrium when most of the pile material is stirred into the background mantle. The changes of the pile morphology and the upper mantle temperature are both gradual processes.

For most cases, we use an initial temperature of $T = 0.72$ or 1800 K if scaled with $\Delta T = 2500$ K, which is consistent with some recent geochemical constrains that the upmost mantle potential temperature is ∼1500–1600 °C at ∼2.5–3.0 Ga (e.g., Herzberg et al., 2010). However, we do not know what the initial temperature configuration of the incipient solid-state mantle was for the true Earth, particularly how it varied radially and laterally. This would largely be controlled by liquid–solid 2-phase convection as the mantle was solidifying and the processes that formed the putative dense layer in the first place (e.g., Ballmer et al., 2017; Labrosse et al., 2007). In fact, for many of the layer-forming processes that have been proposed, one could imagine a very complicated, heterogeneous initial temperature distribution at the time when the mantle first became entirely solid state. Our employment of a uniform temperature across both layers is motivated by trying to design a simple experiment to draw out basic, fundamental principles. Given the straight-forward design of our experiments (homogeneous initial temperature) and the lack of the

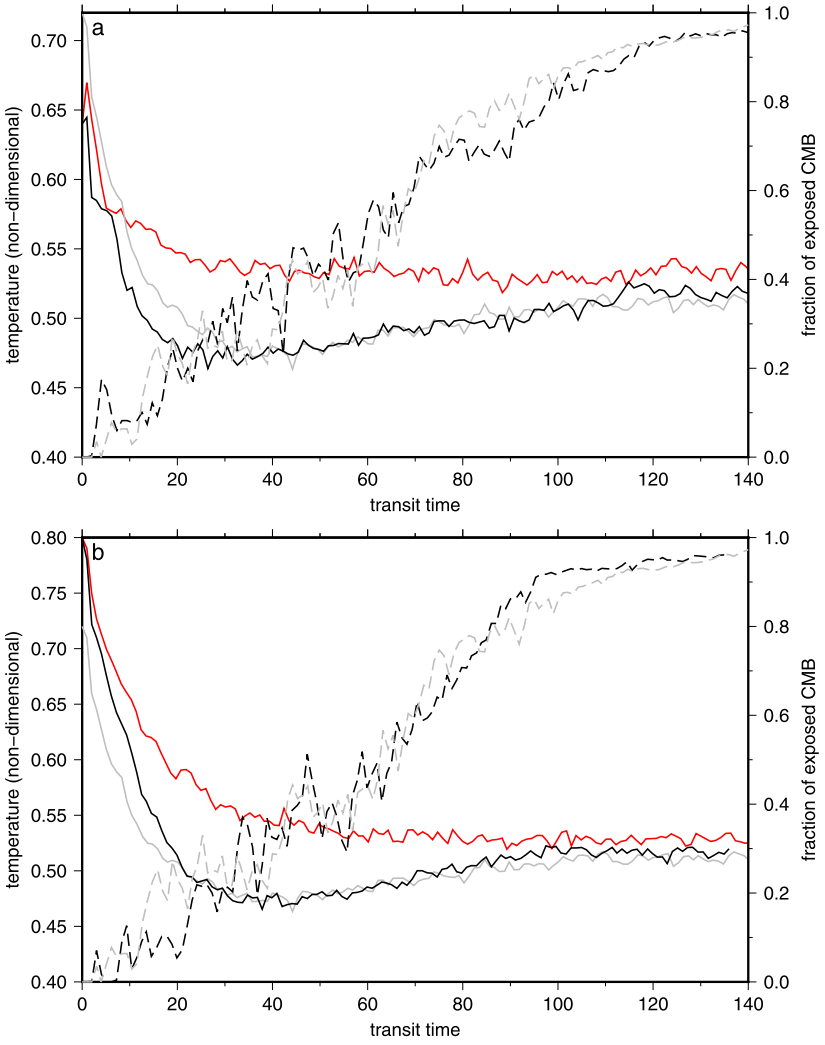

Fig. 8. a, Time evolution of the ambient upper mantle temperature at 300 km depth (T_{300}) for cases ISO5.1 (solid red), TC5.1 (solid black), and TC1.1 (solid gray), and the fraction of exposed CMB not covered by intrinsic dense material for cases TC5.1 (dashed black) and TC1.1 (dashed gray). **b**, Time evolution of the ambient upper mantle temperature at 300 km depth (T_{300}) for cases ISO5.2 (solid red), TC5.2 (solid black), and TC1.1 (solid gray), and the fraction of exposed CMB not covered by intrinsic dense material for cases TC5.2 (dashed black) and TC1.1 (dashed gray). Cases ISO5.1 and TC5.1 have an initial mantle temperature of $T = 0.64$, and cases ISO5.2 and TC5.2 have an initial mantle temperature of $T = 0.8$.

understanding of what the actual temperature state was, one must take caution when interpreting our time scales. For example, our experiments must undergo a transient stage in which lateral temperature gradients are established to drive convection and the temperature of the dense layer on the CMB adjusts to a relatively stable value (Supplementary Information Fig. S2). This transient stage may not occur in the real Earth's mantle. Perhaps for the real Earth, lateral temperature gradients and the relatively stable thermal status of the dense layer were already well-established at the beginning of solid-state convection. Nevertheless, our results show that the initial temperature condition does not affect the long-term evolution of the upper mantle temperature (e.g., Fig. 8). Whatever the initial temperature conditions were, the large-scale compositional heterogeneity on the CMB would insulate the core and therefore, reduce the heat loss coming out of it, as shown by Nakagawa and Tackley (2004). This insulating effect causes mantle temperature to decrease more rapidly than comparable isochemical models. In contrast, the temperature of the dense layer on the CMB is relatively stable (e.g., Supplementary Information Fig. S2). As a consequence, the density contrast between the dense layer and background mantle decreases, and therefore with time, the dense layer is continually gaining more topography and exposing more core surface for the background mantle to come into contact with. The increase of the exposed CMB area causes the increase of CMB heat flux, which in turn results in reduced cooling rate of the background mantle.

We further quantify how fast T_{300} increases with time after it reaches a minimum value. Previous parameterized convection models which take into account the decay of radiogenic heating and the cooling of the Earth's core but do not consider the effects of thermochemical convection in the lowermost mantle suggest a mantle cooling rate of ~30-200 K/Gyr (e.g., Davies, 1993; Davies, 2009; Korenaga, 2006) since the Archean. Petrological constraints suggest that the uppermost mantle potential temperature has decreased by ~100–250 °C since ~3 Ga, with a cooling rate of ~30–90 K/Gyr (Abbott et al., 1994; Grove and Parman, 2004; Herzberg et al., 2010). For better comparison, we convert the non-dimensional temperature used in our geodynamic models to dimensional values using a reference temperature of $\Delta T =$ 2500 K (Table 1), and the transit time is scaled to geological time by assuming that 1 transit time equals to 60 Myr which is similar to previous studies (Christensen and Hofmann, 1994; Li and McNamara, 2013). Table 2 shows the average rate of T_{300} increase within the first ~10 transit time (or ~600 Myr) after T_{300} reaches a minimum, for all thermochemical cases except case TC1.2. This rate of temperature increase ranges from ~46 K/Gyr for

cases TC1.4, to ∼75 K/Gyr for case TC1.1. Since our models assume constant internal heating rate and CMB temperature, the temperature increase in our models is solely caused by the transition from global layer to isolated piles of compositional heterogeneity. This temperature is significant, compared to the secular cooling of the Earth's mantle of 30–200 K/Gyr (e.g., Abbott et al., 1994; Davies, 1993, 2009; Grove and Parman, 2004; Herzberg et al., 2010; Korenaga, 2006). Thus, the gradual increasing of the T_{300} caused by the changes of morphology of compositional heterogeneity in the lowermost mantle could have counteracted, at least partially, the cooling of the mantle due to core cooling and reducing concentration of heat producing elements, which leads to reduced cooling rate of Earth's upper mantle (compared to isochemical models). This reduced cooling rate will persist until the entire thermochemical piles are stirred into the background mantle.

We find that although the details of dynamics vary case by case, all thermochemical cases (except case TC1.2) show the same trends of thermal evolution for the upper mantle. More complex rheology and geodynamical models are possible, but the added complexity leads to added uncertainty. For example, viscosity is dependent on grain-size, but we don't have an understanding of what the average grain size of the lower mantle is, and worse, we don't know how heterogeneous the grain-size distribution is. Furthermore, if a dense-layer exists, we expect it should have, in general, a different grain-size than the background mantle (e.g., Solomatov and Reese, 2008). If the grain-size of the dense material is larger than that of the background mantle, the dense structures can become more dynamically active, better resist entrainment into the background mantle, and have more plume-like morphologies (e.g., McNamara and Zhong, 2004). Nevertheless, our straight-forward experiments highlight that one key factor to the mantle thermal evolution is the fraction of the CMB that is exposed to the background mantle. The longer the intrinsically dense material covers the CMB globally, the more time it takes for the upper mantle temperature to reach its minimum value. Similarly, the longer the pile material stays in the lowermost mantle and covers the CMB, the more time it takes for the upper mantle temperature to increase to a relatively stable values.

As is shown in our models (Fig. 1), the global layer of dense material is pushed into isolated piles by the subducted downwellings (e.g., slabs). Before plate tectonics initiated, it is likely that thermal downwellings were not nearly as negatively buoyant as the lithospheric slab downwellings inherent in plate tectonics. It is therefore possible that the onset of plate tectonic, with the resultant change from weak thermal downwellings to denser, lithospheric slab downwellings, could have punctuated the transition from a global layer to isolated piles. The actual time lag from the start of plate tectonics to the reduced cooling rate due to the change of pile morphology would depend on how fast the subducted slabs could reach the lowermost mantle and, more importantly, on how efficiently the slabs push the global layer of dense material into isolated piles. Specifically, the present-day Earth's lowermost mantle is featured by two isolated LLSVPs. Assuming that the LLSVPs are caused by primordial thermochemical piles, our results suggest that the size of the LLSVPs may be decreasing due to entrainment. Therefore, the CMB heat flux for the present-day Earth may be increasing, and as a result, the upper mantle may be cooling slower than before, or even warming up.

In this study, the large-scale compositional heterogeneity is assumed to be caused by remnants of Earth's early differentiation. However, there are other hypotheses for the origin compositional heterogeneity, such as accumulation of subducted oceanic crust on the CMB (e.g., Brandenburg and van Keken, 2007; Christensen and Hofmann, 1994; Davies, 2008; Mulyukova et al., 2015; Tolstikhin and Hofmann, 2005). Our previous study (Li and McNamara, 2013) has demonstrated that for thin, 6 km thick oceanic crust under present-day Earth's condition, the bulk of the crust is easily stirred into the background mantle and it is therefore difficult for thin subducted oceanic crust to accumulate into large piles on the CMB, comparable to the size of LLSVPs. Mulyukova et al. (2015) found conflicting results and showed that the subducted oceanic crust could segregate to the CMB and accumulate into large thermochemical piles similar in shape to the LLSVPs. The oceanic crust is suggested to be thicker in the early hotter Earth (e.g., McKenzie and Bickle, 1988; Su et al., 1994). When did the plate tectonics start is a matter of great debate. However, if there was subduction during the early hotter Earth, the thick subducted oceanic crust could accumulate on the CMB more easily (e.g., Christensen and Hofmann, 1994; Nakagawa and Tackley, 2014; Nakagawa et al., 2009; Tackley, 2011). Campbell and Griffiths (2014) proposed that large accumulations of subducted oceanic crust formed a global layer on the CMB at the end of Archean, which could have led to a rapid decrease in mantle plume temperature. Our results indicate that a global layer of subducted oceanic crust could also lead to rapid cooling of upper mantle. If the thickness of subducted oceanic crust decreases with the cooling of the upper mantle, at some point, the volume of accumulated oceanic crust in the lowermost mantle would stop increasing, and the subducted oceanic crust would be pushed by cold dowenwellings (e.g., slabs) into isolated thermochemical piles which are slowly entrained and mixed into the background mantle. This process could lead to gradual temperature increases or decreased cooling rate of the ambient mantle. It may also increase the temperature of mantle plumes because mantle plumes forming on the exposed CMB are predicted to be hotter than that forming on top of the global dense layer (Farnetani, 1997; Li and Zhong, 2017; Tan et al., 2011).

In conclusion, we show that the long-term existence of large-scale compositional heterogeneity in the Earth's lowermost mantle plays significant role in Earth's thermal evolution. The transition from global layer of intrinsically dense compositional heterogeneity to isolated thermochemical piles, and later the decreasing volume of these piles by entrainment could lead to reduced cooling rate, or perhaps gradual temperature increase, of the upper mantle in Earth's history. This effect should be considered in future work involved with understanding Earth's thermal evolution.

Acknowledgements

This work was funded by NSF grants EAR-1338810 and EAR-1722623.

Appendix A. Supplementary material

Supplementary material related to this article can be found online at https://doi.org/10.1016/j.epsl.2018.08.009.

References

Abbott, D., Burgess, L., Longhi, J., Smith, W.H.F., 1994. An empirical thermal history of the Earth's upper mantle. J. Geophys. Res. 99, 13835–13850. https://doi.org/10.1029/94JB00112.

Ballmer, M.D., Lourenco, D.L., Hirose, K., Caracas, R., Nomura, R., 2017. Reconciling magma-ocean crystallization models with the present-day structure of the Earth's mantle. Geochem. Geophys. Geosyst. 18, 2785–2806. https://doi.org/10.1002/2017gc006917.

Brandenburg, J.P., van Keken, P.E., 2007. Deep storage of oceanic crust in a vigorously convecting mantle. J. Geophys. Res. 112, B06403. https://doi.org/10.1029/2006jb004813.

Campbell, I.H., Griffiths, R.W., 2014. Did the formation of D″ cause the Archaean–Proterozoic transition? Earth Planet. Sci. Lett. 388, 1–8. https://doi.org/10.1016/j.epsl.2013.11.048.

Christensen, U.R., 1985. Thermal evolution models for the Earth. J. Geophys. Res. 90, 2995–3007. https://doi.org/10.1029/JB090iB04p02995.

Christensen, U.R., Hofmann, A.W., 1994. Segregation of subducted oceanic crust in the convecting mantle. J. Geophys. Res. 99, 19867–19884. https://doi.org/10.1029/93JB03403.

Coltice, N., Phillips, B.R., Bertrand, H., Ricard, Y., Rey, P., 2007. Global warming of the mantle at the origin of flood basalts over supercontinents. Geology 35, 391–394. https://doi.org/10.1130/g23240a.1.

Davaille, A., 1999. Simultaneous generation of hotspots and superswells by convection in a heterogenous planetary mantle. Nature 402, 756–760. https://doi.org/10.1038/45461.

Davies, G.F., 1980. Thermal histories of convective Earth models and constraints on radiogenic heat production in the Earth. J. Geophys. Res. 85, 2517–2530. https://doi.org/10.1029/JB085iB05p02517.

Davies, G.F., 1993. Cooling the core and mantle by plume and plate flows. Geophys. J. Int. 115, 132–146. https://doi.org/10.1111/j.1365-246X.1993.tb05593.x.

Davies, G.F., 2008. Episodic layering of the early mantle by the 'basalt barrier' mechanism. Earth Planet. Sci. Lett. 275, 382–392. https://doi.org/10.1016/j.epsl.2008.08.036.

Davies, G.F., 2009. Effect of plate bending on the Urey ratio and the thermal evolution of the mantle. Earth Planet. Sci. Lett. 287, 513–518. https://doi.org/10.1016/j.epsl.2009.08.038.

Deschamps, F., Kaminski, E., Tackley, P.J., 2011. A deep mantle origin for the primitive signature of ocean island basalt. Nat. Geosci. 4, 879–882. https://doi.org/10.1038/Ngeo1295.

Farnetani, C.G., 1997. Excess temperature of mantle plumes: the role of chemical stratification across D″. Geophys. Res. Lett. 24, 1583–1586. https://doi.org/10.1029/97gl01548.

Franck, S., 1998. Evolution of the global mean heat flow over 4.6 Gyr. Tectonophysics 291, 9–18. https://doi.org/10.1016/S0040-1951(98)00027-4.

Grove, T.L., Parman, S.W., 2004. Thermal evolution of the Earth as recorded by komatiites. Earth Planet. Sci. Lett. 219, 173–187. https://doi.org/10.1016/S0012-821X(04)00002-0.

Hernlund, J.W., Tackley, P.J., 2008. Modeling mantle convection in the spherical annulus. Phys. Earth Planet. Inter. 171, 48–54. https://doi.org/10.1016/j.pepi.2008.07.037.

Herzberg, C., Condie, K., Korenaga, J., 2010. Thermal history of the Earth and its petrological expression. Earth Planet. Sci. Lett. 292, 79–88. https://doi.org/10.1016/j.epsl.2010.01.022.

Honda, S., 1995. A simple parameterized model of Earth's thermal history with the transition from layered to whole mantle convection. Earth Planet. Sci. Lett. 131, 357–369. https://doi.org/10.1016/0012-821X(95)00034-A.

Korenaga, J., 2006. Archean geodynamics and the thermal evolution of Earth. In: Benn, J.-C.M., Condie, K. (Eds.), AGU Geophysical Monograph Series. AGU, Washington, DC, pp. 7–32.

Labrosse, S., Hernlund, J.W., Coltice, N., 2007. A crystallizing dense magma ocean at the base of the Earth's mantle. Nature 450, 866–869. https://doi.org/10.1038/Nature06355.

Lenardic, A., Moresi, L., Jellinek, A.M., O'Neill, C.J., Cooper, C.M., Lee, C.T., 2011. Continents, supercontinents, mantle thermal mixing, and mantle thermal isolation: theory, numerical simulations, and laboratory experiments. Geochem. Geophys. Geosyst. 12, Q10016. https://doi.org/10.1029/2011gc003663.

Li, M., McNamara, A.K., 2013. The difficulty for subducted oceanic crust to accumulate at the Earth's core–mantle boundary. J. Geophys. Res. 118, 1807–1816. https://doi.org/10.1002/Jgrb.50156.

Li, M., McNamara, A.K., Garnero, E.J., 2014. Chemical complexity of hotspots caused by cycling oceanic crust through mantle reservoirs. Nat. Geosci. 7, 366–370. https://doi.org/10.1038/Ngeo2120.

Li, X.D., Romanowicz, B., 1996. Global mantle shear velocity model developed using nonlinear asymptotic coupling theory. J. Geophys. Res. 101, 22245–22272. https://doi.org/10.1029/96JB01306.

Li, M., Zhong, S., 2017. The source location of mantle plumes from 3D spherical models of mantle convection. Earth Planet. Sci. Lett. 478, 47–57. https://doi.org/10.1016/j.epsl.2017.08.033.

McKenzie, D., Bickle, M.J., 1988. The volume and composition of melt generated by extension of the lithosphere. J. Petrol. 29, 625–679. https://doi.org/10.1093/petrology/29.3.625.

McNamara, A.K., Keken, P.E.v., 2000. Cooling of the Earth: a parameterized convection study of whole versus layered models. Geochem. Geophys. Geosyst. 1. https://doi.org/10.1029/2000gc000045.

McNamara, A.K., Zhong, S., 2005. Thermochemical structures beneath Africa and the Pacific Ocean. Nature 437, 1136–1139. https://doi.org/10.1038/nature04066.

McNamara, A.K., Zhong, S.J., 2004. Thermochemical structures within a spherical mantle: superplumes or piles? J. Geophys. Res. 109, B07402. https://doi.org/10.1029/2003jb002847.

Mulyukova, E., Steinberger, B., Dabrowski, M., Sobolev, S.V., 2015. Survival of LLSVPs for billions of years in a vigorously convecting mantle: replenishment and destruction of chemical anomaly. J. Geophys. Res. 120, 3824–3847. https://doi.org/10.1002/2014jb011688.

Nakagawa, T., Tackley, P.J., 2004. Effects of thermo-chemical mantle convection on the thermal evolution of the Earth's core. Earth Planet. Sci. Lett. 220, 107–119. https://doi.org/10.1016/S0012-821x(04)00055-X.

Nakagawa, T., Tackley, P.J., 2012. Influence of magmatism on mantle cooling, surface heat flow and Urey ratio. Earth Planet. Sci. Lett. 329–330, 1–10. https://doi.org/10.1016/j.epsl.2012.02.011.

Nakagawa, T., Tackley, P.J., 2014. Influence of combined primordial layering and recycled MORB on the coupled thermal evolution of Earth's mantle and core. Geochem. Geophys. Geosyst. 15, 619–633. https://doi.org/10.1002/2013GC005128.

Nakagawa, T., Tackley, P.J., Deschamps, F., Connolly, J.A.D., 2009. Incorporating self-consistently calculated mineral physics into thermochemical mantle convection simulations in a 3-D spherical shell and its influence on seismic anomalies in Earth's mantle. Geochem. Geophys. Geosyst. 10, Q03004. https://doi.org/10.1029/2008gc002280.

Phillips, B.R., Bunge, H.-P., 2005. Heterogeneity and time dependence in 3D spherical mantle convection models with continental drift. Earth Planet. Sci. Lett. 233, 121–135. https://doi.org/10.1016/j.epsl.2005.01.041.

Ritsema, J., van Heijst, H.J., Woodhouse, J.H., 2004. Global transition zone tomography. J. Geophys. Res. 109, B02302. https://doi.org/10.1029/2003jb002610.

Schubert, G., Stevenson, D., Cassen, P., 1980. Whole planet cooling and the radiogenic heat source contents of the Earth and Moon. J. Geophys. Res. 85, 2531–2538. https://doi.org/10.1029/JB085iB05p02531.

Solomatov, V., Reese, C., 2008. Grain size variations in the Earth's mantle and the evolution of primordial chemical heterogeneities. J. Geophys. Res. https://doi.org/10.1029/2007JB005319.

Sotin, C., Labrosse, S., 1999. Three-dimensional thermal convection in an iso-viscous, infinite Prandtl number fluid heated from within and from below: applications to the transfer of heat through planetary mantles. Phys. Earth Planet. Inter. 112, 171–190. https://doi.org/10.1016/S0031-9201(99)00004-7.

Su, W., Mutter, C.Z., Mutter, J.C., Buck, W.R., 1994. Some theoretical predictions on the relationships among spreading rate, mantle temperature, and crustal thickness. J. Geophys. Res. 99, 3215–3227. https://doi.org/10.1029/93JB02965.

Tackley, P., 1998. Three-dimensional simulations of mantle convection with a thermo-chemical basal boundary layer: D″. In: Gurnis, M. (Ed.), AGU Geophysical Mongraph on the CMB.

Tackley, P.J., 2011. Living dead slabs in 3-D: the dynamics of compositionally-stratified slabs entering a "slab graveyard" above the core–mantle boundary. Phys. Earth Planet. Inter. 188, 150–162. https://doi.org/10.1016/j.pepi.2011.04.013.

Tackley, P.J., King, S.D., 2003. Testing the tracer ratio method for modeling active compositional fields in mantle convection simulations. Geochem. Geophys. Geosyst. 4, 8302. https://doi.org/10.1029/2001gc000214.

Tan, E., Leng, W., Zhong, S.J., Gurnis, M., 2011. On the location of plumes and lateral movement of thermochemical structures with high bulk modulus in the 3-D compressible mantle. Geochem. Geophys. Geosyst. 12, Q07005. https://doi.org/10.1029/2011gc003665.

Tolstikhin, I., Hofmann, A.W., 2005. Early crust on top of the Earth's core. Phys. Earth Planet. Inter. 148, 109–130. https://doi.org/10.1016/j.pepi.2004.05.011.

Zhang, N., Zhong, S.J., 2011. Heat fluxes at the Earth's surface and core–mantle boundary since Pangea formation and their implications for the geomagnetic superchrons. Earth Planet. Sci. Lett. 306, 205–216. https://doi.org/10.1016/j.epsl.2011.04.001.

Zhang, N., Zhong, S., Leng, W., Li, Z.-X., 2010. A model for the evolution of the Earth's mantle structure since the Early Paleozoic. J. Geophys. Res. 115, B06401. https://doi.org/10.1029/2009jb006896.

Zhong, S., 2006. Constraints on thermochemical convection of the mantle from plume heat flux, plume excess temperature, and upper mantle temperature. J. Geophys. Res. 111, B04409. https://doi.org/10.1029/2005jb003972.

Zhong, S.J., Gurnis, M., 1993. Dynamic feedback between a continentlike raft and thermal convection. J. Geophys. Res. 98, 12219–12232. https://doi.org/10.1029/93jb00193.